Journal of Geophysical Research: Earth Surface

RESEARCH ARTICLE
10.1029/2017JF004541

Evolving Environmental and Geometric Controls on Columbia Glacier's Continued Retreat

Ellyn M. Enderlin[1,2], Shad O'Neel[3], Timothy C. Bartholomaus[4], and Ian Joughin[5]

[1]Climate Change Institute, University of Maine, Orono, ME, USA, [2]School of Earth and Climate Sciences, University of Maine, Orono, ME, USA, [3]USGS Alaska Science Center, Anchorage, AK, USA, [4]Department of Geological Sciences, University of Idaho, Moscow, ID, USA, [5]Applied Physics Laboratory, University of Washington, Seattle, WA, USA

Key Points:
- Although Columbia Glacier's long-term retreat drove acceleration, seasonal terminus position and speed change are not necessarily linked
- The primary controls on frontal ablation vary with terminus geometry, which must be accounted for when modeling dynamic change
- Seasonal meltwater-driven changes in basal drag can exert a stronger control over ice flow speed than changes in terminus position

Supporting Information:
- Supporting Information S1

Correspondence to:
E. M. Enderlin,
ellyn.enderlin@gmail.com

Citation:
Enderlin, E. M., O'Neel, S., Bartholomaus, T. C., & Joughin, I. (2018). Evolving environmental and geometric controls on Columbia Glacier's continued retreat. *Journal of Geophysical Research: Earth Surface*, *123*, 1528–1545. https://doi.org/10.1029/2017JF004541

Received 7 NOV 2017
Accepted 25 MAY 2018
Accepted article online 11 JUN 2018
Published online 10 JUL 2018

Abstract Geometry strongly controls the dynamic behavior of marine-terminating (tidewater) glaciers, significantly influencing advance and retreat cycles independent of climate. Yet the recent, nearly ubiquitous retreat of tidewater glaciers suggests that changes in atmospheric and oceanic forcing may also drive dynamic change. To isolate the influence of geometry on tidewater glacier dynamics, we analyzed detailed observational time series from 2012 to 2016 for two tidewater glaciers with shared dynamic histories and environmental forcing: Columbia Glacier and its former tributary (Post Glacier) in southcentral Alaska. We find that although terminus retreat has driven decadal-scale changes in dynamics of the Columbia-Post system, environmental factors contribute to short-term (i.e., seasonal) dynamic variability. In particular, analysis of force balance time series indicates that observed variations in speed result from seasonal changes to the subglacial hydrologic system and associated changes in basal drag. Variations in terminus position only drive noticeable speed change when the terminus retreats from regions of relatively high basal drag. In agreement with long-term analyses of Columbia Glacier, we find that terminus geometry can perturb the timing of seasonal ice flow patterns. Specifically, our data support the idea that retreat of a glacier terminus into deeper water is accompanied by a shift in the primary control on frontal ablation. Although our analysis focuses on two Alaskan glaciers, our data suggest that changes in the relative importance of surface meltwater and buoyancy effects on submarine melting and/or calving may manifest as a shift in terminus change seasonality and offer a mechanism to identify frontal ablation controls.

Plain Language Summary Over the last two decades, glaciers that flow into the ocean (i.e., marine-terminating glaciers) have largely retreated in response to changes in climate. However, the amount by which climate forces glacier change is strongly controlled by glacier and fjord shape. Therefore, the same amount of climate change can lead to differences in the timing and magnitude of glacier flow and length change. In this paper, we investigate differences in recent glacier change at two formerly merged glaciers in southcentral Alaska: Columbia Glacier and its western tributary, Post Glacier. We find that the multidecadal correlations between length change and speed break down over seasonal time scales and that seasonal changes in glacier speed are related to the way water flows beneath the glacier. Furthermore, we find that glacier size and shape influence the seasonal controls on terminus position, resulting in variable seasonal patterns of glacier length and ice flow. While our study focuses on two of many marine-terminating glaciers worldwide, we suggest that (1) glacier shape modulates the influence of air and ocean temperature change on ice flow and iceberg production and (2) studies of glacier change and its drivers should ensure that subseasonal changes in glacier speed and length are resolved.

1. Introduction

Increases in dynamic mass loss from marine-terminating glaciers over the last two decades have sparked a growing concern over future mass loss from glaciers and ice sheets and the associated impacts on global sea level and ocean circulation (Enderlin et al., 2014; Gardner et al., 2018; McNabb et al., 2015; Mouginot et al., 2014; Rott et al., 2011; van den Broeke et al., 2016; Van Wychen et al., 2015). Although enhanced dynamic mass loss has occurred throughout the Arctic and Antarctic, the timing and magnitude of changes in glacier dynamics have varied over a range of spatial scales (Carr et al., 2013, 2014, 2015; Enderlin et al., 2014; Gardner et al., 2018; Jamieson et al., 2012; Porter et al., 2014). A portion of the observed glacier variability can be explained by differences in environmental forcing (i.e., external controls, such as surface and submarine melting and iceberg calving). However, differences in glacier geometry (internal control) also modulate the dynamic response of marine-terminating glaciers to climate change (Enderlin et al., 2013). In

fact, geometry can exert such a profound control over glacier dynamics that tidewater (i.e., grounded and marine-terminating) glaciers progress through cycles of terminus advance and retreat even under steady climatic conditions (Brinkerhoff et al., 2017; Clarke, 1987; Post, 1975).

As originally described in Alaska, these alternating periods of slow tidewater glacier advance (lasting ~1,000 years) and rapid terminus retreat (~100 years) are known as the "tidewater glacier cycle" (Meier & Post, 1987). The classical view of the tidewater glacier cycle holds that climate plays a weak role in tidewater glacier advance and retreat (Meier & Post, 1987; Post, 1975) and that, especially during retreat, glacier behavior is independent of the climatic mass balance (Pfeffer, 2007). However, if the advance and retreat phases of the tidewater glacier cycle are truly independent of climate, then the vast majority of tidewater glaciers should be advancing at any given time (Brinkerhoff et al., 2017; IPCC, 2013; Post et al., 2011). This expectation is inconsistent with observations of widespread tidewater glacier retreat throughout the Arctic (Carr et al., 2017), even in Greenland (Howat & Eddy, 2011), where the vast interior ice sheet reservoir enables quick recovery of glaciers from retreat (Howat et al., 2011; Joughin et al., 2008).

Both observation and model-based investigations are challenged by the complexity of tidewater glacier environments and behavior, and as such, our scientific understanding of retreat processes and drivers remains limited. Here we analyze approximately monthly, ~15–300 m resolution remote sensing data acquired between 2012 and 2016 at Alaska's Columbia Glacier. Our analysis helps to better resolve the relative importance of internal and external controls on retreating tidewater glaciers over seasonal to interannual time scales. Beginning ca. 2010, two of Columbia Glacier's primary tributaries dynamically, then physically, decoupled into independent glaciers (Figures 1a and 1b). To distinguish the recently decoupled branches, we refer to the former West Branch as Post Glacier and the main and east branches and the main trunk downstream of their confluence as Columbia Glacier. We focus our analysis on these recently decoupled glaciers, with both shared dynamic histories and shared environmental forcings, because they offer an ideal opportunity to explore the importance of glacier geometry to the exclusion of other potentially important variables. Our remote sensing record offers insight with unprecedented temporal and spatial resolutions.

2. Setting

Columbia Glacier is one of southcentral Alaska's largest tidewater glaciers (910 km^2 in 2011; McNabb et al., 2012). This glacier has long been considered the archetype for the retreat phase of the tidewater glacier cycle (e.g., Meier & Post, 1987; Post et al., 2011). Columbia Glacier began its now ~35 yearlong retreat in the early 1980s (Meier & Post, 1987; Figures 1a and 1b), marking the end of a $>$200 yearlong period of terminus stability (Barclay et al., 2009; Calkin et al., 2001; Carlson et al., 2017; Vancouver, 1798). The rates of retreat and frontal ablation have evolved over time, not necessarily in step (Krimmel, 2001). For example, the retreat rate slowed while frontal ablation remained high in the early 2000s as the glacier terminus passed through a constriction in the fjord (Boldt Love et al., 2016), then accelerated again in the late 2000s when the terminus retreated into the wider and deeper inner fjord (Figures 1a and 1b; Walter et al., 2010). Inspection of the satellite image record indicates that their respective retreat rates diverged following the dynamic and physical decoupling of the two primary tributary glaciers ca. 2010: Columbia Glacier maintained a stable position from ~2010 to 2013, but retreat rates approached 1 km yr^{-1} for Post Glacier over the same time period. Rapid retreat of Columbia Glacier resumed in 2014 and continued through summer 2017, whereas retreat of Post slowed over the same time interval. This disparate behavior suggests that the influence of geometry on the glaciers' continued demise can override local, environmental forcing during retreat.

3. Methods

We combined 72 terminus positions, 89 velocity fields, and 31 digital elevation models (DEMs) acquired between 2012 and 2016 to quantify and assess dynamic and geometric changes at Columbia and Post Glaciers (Figure S1 in the supporting information). Precise synchronization of these temporally independent observational data sets allows us to resolve time series of ice flux and force balance.

3.1. Observational Data

Ice surface velocities were computed from TerraSAR-X and TanDEM-X SAR data, using standard speckle-tracking methods (Joughin, 2002). The 100-m posted (true resolution is ~300 m) velocities were

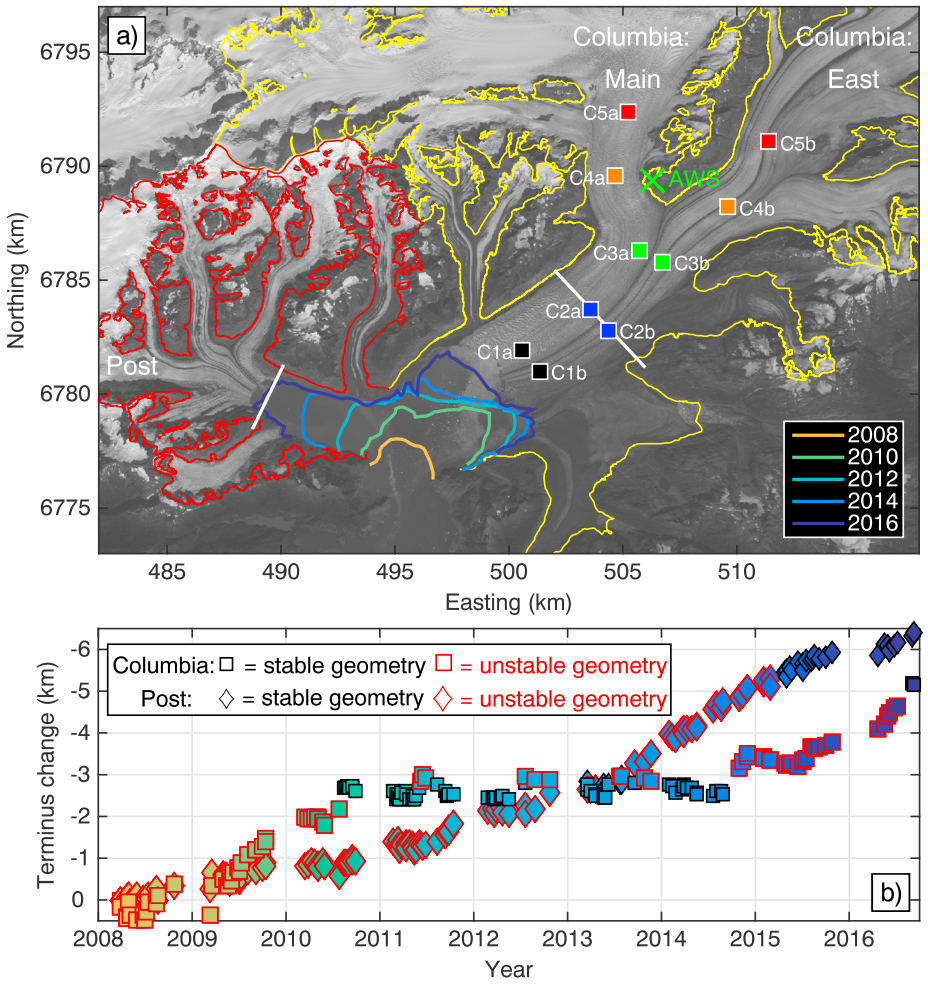

Figure 1. (a) Locations of 2008–2016 biannual terminus positions (colored curves), fluxgates (white straight lines) used for dynamic flux calculations, and stress time series (colored squares) overlain on a Landsat 8 panchromatic image from 31 August 2016. The green "X" marks the location of an automated weather station. The yellow and red glacier outlines for Columbia and Post Glaciers, respectively, were obtained from the Global Land Ice Measurements from Space Glacier Database (Cogley et al., 2015). (b) Centerline terminus position change since 2008 for Columbia and Post Glaciers. Negative values indicate terminus retreat. The larger symbols with red outlines indicate that the terminus geometry did not satisfy the stability criterion (i.e., thickness/water depth $>$ 1.49) of Pfeffer (2007). The same color scheme is used for the terminus traces in (a) and symbol faces in (b).

resampled to the 150-m resolution bed elevation map postings using a linear distance-weighted approach (Enderlin et al., 2016).

Surface elevations were extracted from panchromatic stereo images collected by the DigitalGlobe WorldView satellites. High-resolution (2 m) DEMs were produced from the stereo images (Shean et al., 2016) and vertically coregistered using bedrock outcrops spanning the near-terminus regions of both glacier tributaries. Following coregistration, DEMs were downsampled to the common 150-m postings using a linear distance-weighted approach, which also smooths the data and minimizes random errors (Enderlin et al., 2016). Manual inspection of the 2-m resolution DEMs indicates that horizontal offsets between DEMs are a few pixels or less and have negligible influence on surface elevations extracted from the downsampled DEMs, particularly in the low-slope regions that are the focus of our analysis.

To extend the 1952–2012 record of Columbia Glacier terminus positions by McNabb and Hock (2014), which is derived from historical topographic maps and Landsat images, we manually digitized terminus positions from 2013 to 2016 in cloud-free Landsat 7 and 8 panchromatic images. Terminus positions could also be delineated from the available TerraSAR-X and TanDEM-X SAR imagery, as in Vijay and Braun (2017).

A comparison of 2012 and 2013 terminus position time series constructed from Landsat imagery and from TerraSAR-X/TanDEM-X SAR imagery indicates that the seasonal to interannual patterns of terminus position change of interest here are captured equally well by the two satellite platforms. Therefore, we choose to map terminus positions using Landsat imagery in order to extend the long-term record of McNabb and Hock (2014) using a consistent observational data set (i.e., Landsat images) during the satellite era.

3.2. Bed Elevation Estimates

We merged the two most recent mass-conserving bed-elevation maps constructed for Columbia Glacier (Enderlin et al., 2016; McNabb et al., 2012) and further refined the composite bedmap using a flotation-based criterion over the recently opened inner fjord (Figure 1a). The bed elevation map from McNabb et al. (2012), hereafter called the M12 bedmap, covers the entirety of the Columbia and Post catchment areas but is only loosely constrained by radar-derived bed elevation observations. McNabb et al. (2012) estimated an average bias of ~5 m between their bed elevation estimates and the true bed elevation and an uncertainty (i.e., random error) of 47 m. Comparisons of the M12 bedmap with newer sonar-derived fjord depths (Campbell, 2014) and decluttered and reprocessed radar profiles indicate that the true bed is deeper than the M12 bedmap by an average of ~115 m in the inner fjord and ~2 m beneath Columbia's trunk (i.e., from the 2012 terminus to C5a/b in Figure 1) and that residuals are not randomly distributed over the glacier length (Figure S2).

The more recent mass-conserving bedmap from Enderlin et al. (2016; E16 bedmap) incorporates decluttered and reprocessed radar profiles collected during 2012 (Rignot et al., 2013) that are less prone to errors than the earlier radar observations available to McNabb et al. (2012). However, this more accurate map only covers the trunk of Columbia Glacier over the lowest ~10 km of its two major tributaries (Figure 2a); Post Glacier is not included in this product.

The limited spatial extent of the updated bedmap and apparent near-terminus bias of the M12 bedmap motivates refined bed-depth estimates through the inner fjord, which we approached using a flotation criterion. We estimated bed elevations, z_b, between pairs of terminus positions assuming that the ice between the terminus observation dates (~3 weeks) calved when the glacier thickness (H) dropped below a critical fraction above the flotation thickness (H_f; Nick et al., 2007; Vieli et al., 2001). According to this criterion, which was inspired by and developed using observations from Columbia Glacier, ice calves when

$$H \leq 1.15 H_f. \tag{1}$$

Equation (1) can be rewritten in terms of the bed and surface elevations such that calving occurs when

$$z_s - z_b \leq -1.15 \frac{\rho_{sw}}{\rho_i} z_b, \tag{2}$$

where z_s is the ice surface elevation, z_b is the bed elevation, and ρ_{sw} and ρ_i are the density of seawater (1,026 kg m^{-3}) and ice (900 kg m^{-3}), respectively. Equation (2) was rearranged so that bed depth estimates were computed using ice surface elevation estimates between all possible terminus pairs, then averaged (standard deviation of stacked estimates was $<$1 m) in regions of spatial overlap (i.e., regions of temporary terminus readvance). Gaps in the flotation-based bed map were filled via linear interpolation, and the complete bedmap was smoothed using a 3 pixel-wide (450 m) moving area window to minimize noise. The final flotation-based bedmap is more accurate than the M12 bedmap overall, with average offsets of +43 m in the inner fjord (over-estimated bed elevations relative to sonar) and $-$16 m beneath the glacier (underestimates bed elevations relative to the E16 bedmap), respectively (Figure S2).

The final bedmap spanning the entire Columbia-Post catchment (Figure 2) represents a mosaic of the three bedmaps, using a hierarchy structured by the magnitudes of uncertainty and bias. Preference thus goes first to the E16 bedmap followed by the flotation-based and finally to the M12 bedmap. To smoothly transition between the three bedmaps, we applied a distance-weighted averaging approach across 900 m wide buffers at the edges of each bed map (Figure 2d). The size of the smoothing window was selected to preserve the deepest bed elevations while maintaining a realistic cross-sectional shape for Post Glacier where the bedmaps differed by up to ~400 m.

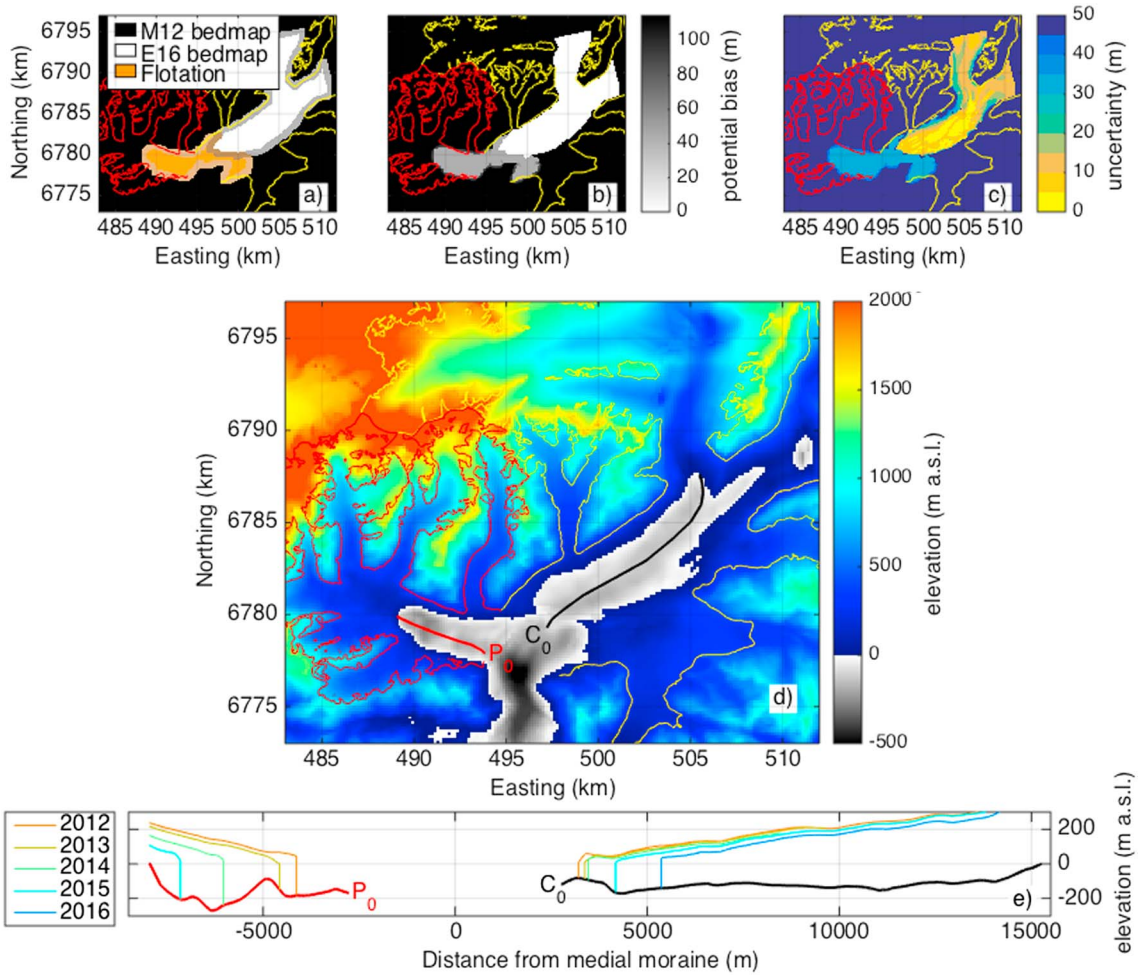

Figure 2. Maps of (a) mosaic masks, (b) potential biases, (c) estimated random errors, and (d) the final mosaicked bed elevations. The thin yellow and red lines in (a)–(d) outline the Columbia and Post Glacier extents. The white and orange colors in (a) correspond to the locations where the updated mass conserving bedmap and flotation-based bedmap were given preference in the mosaic. Bedmaps were smoothed over the light gray and light brown regions. Biases in (b) were estimated from a comparison of bedmap elevations with a sonar-derived bed elevation transect. The bias in the M12 bedmap in (b) should be treated as a conservative estimate because M12 bedmap biases over Columbia's fast-flowing trunk are near zero. The black and red lines in (d) trace the central flowlines of Columbia and Post, respectively, where the glaciers are grounded below sea level. The bed elevation profiles extracted along the centerlines are shown in (e). The thin lines in (e) show annual spring surface elevation profiles along the glacier centerlines.

3.3. Glacier Volume Change Estimates

Glacier volume change can be partitioned into surface mass balance and frontal ablation. Here we focus on frontal ablation, which is composed of two components: (1) change in the thickness and speed of ice flowing toward the terminus and (2) change in glacier length. We refer to these components as the dynamic flux and terminus change flux, respectively.

We calculated the dynamic flux using a fluxgate approach (Figure 1a), in which the product of the ice thickness and speed perpendicular to the gate was integrated over the length of each fluxgate. Flux gate locations were selected to minimize the effects of the time-varying near-terminus force balance on ice flow speeds and to minimize the effects of potential bed elevation biases on ice thickness estimates. We assumed that deformation velocities are negligible relative to basal sliding velocities (O'Neel et al., 2005; Rasmussen, 1989) and adopted the surface speed as a proxy for the depth-averaged speed. For each velocity field, a coincident surface elevation field was obtained by linearly interpolating between the two temporally adjacent DEMs. Ice thickness was estimated as the difference between the time-synchronized surface elevations and bed elevations. We filled gaps in the speed and thickness cross sections by scaling measurements adjacent to gaps by time-averaged, normalized speed and thickness cross sections, which preserves the observed

profile shape (McNabb et al., 2015). Ablation between the fluxgate and terminus was estimated using a positive degree-day model. We combined lapse-adjusted air temperature observations from an ice marginal U.S. Geological Survey-maintained meteorological station (Figure 1a) from August 2012 to 2016 with temperatures recorded in nearby Valdez (~35 km to the east) from January 2012 through present. The degree-day factor used to convert air temperatures to surface ablation rates was obtained from Rasmussen et al. (2011). Given the strongly negative surface mass balance observed below ~1,000 m above sea level at Columbia (Rasmussen et al., 2011), we do not attempt to account for episodic snowfall events in our dynamic flux estimates.

Terminus position changes can substantially contribute to frontal ablation during periods of rapid change (McNabb et al., 2015). Therefore, to construct time series of terminus change fluxes, we integrated the estimated ice thickness fields over the area of terminus change at ~3-week intervals (consistent with velocity field sampling). Because terminus positions were not coincidently sampled with velocity measurements, we linearly interpolated the more slowly varying dynamic flux estimates to the times available for terminus change, to yield approximately 21 measurements of frontal ablation per year.

3.4. Uncertainties

Frontal ablation uncertainties were estimated as the sum of uncertainties from the dynamic flux and terminus volume change terms. Primary error sources include uncertainties in flow speed, surface and bed elevations, and terminus positions. Speed uncertainties were estimated from local variations in ice velocity (i.e., random errors), with an additional 3% uncertainty associated with potential nonsurface-parallel ice flow (Joughin et al., 2010). To verify our assumption that deformation velocities are negligible relative to basal sliding velocities (i.e., depth-averaged speeds = surface speeds), we estimated the deformational velocity as

$$U_d = \frac{1}{2} A H \tau_d^3, \tag{3}$$

where $A = 2.4 \times 10^{-24} \mathrm{Pa}^{-3} \mathrm{s}^{-1}$ is the rate factor for temperate ice, H is the ice thickness (m), and τ_d is the gravitational driving stress (Pa; see section 4.3). The deformational velocity was $<2\%$ of the velocity along the fast-flowing trunks, on average, which is well within our velocity uncertainty estimates. Uncertainties were generally largest near the lateral margins of Post and along the centerline of the fast-flowing main branch for Columbia, with median values in these regions of 0.43 and 0.32 m d^{-1}, respectively.

Surface elevation uncertainties were conservatively estimated from the range in surface elevations of the two temporally bounding DEMs. Although our DEMs have the sparsest temporal coverage of our observational data sets (Figure S1), the average time separation of 54 days between DEMs led to relatively small elevation uncertainties. The average change in centerline ice thickness between consecutive DEMs was ~1–2 m, with maxima of 3.8 m for Columbia and 19.7 m for Post. We obtained uncertainty estimates in the M12 and E16 bedmaps directly from the model output. Although the M12 bedmap appears to be biased over the inner fjord, a comparison of the M12 bed elevations with the available observational (sonar and radar) data suggests that the bedmap's quoted uncertainty of ~47 m is approximately equal to the median of the absolute deviation in bed elevations and therefore provides a reasonable estimate of uncertainty. Where the flotation-based bedmap is used, we use the median of the absolute deviation between the flotation-based bed elevations and sonar-derived bed elevations of ~31 m as our uncertainty estimate (Figure S2). Thickness uncertainties were calculated as the sum of the surface and bed elevation uncertainties. Thickness interpolation onto the times of velocity observations contributes no more than a few percent uncertainty to our calculations due to their small relative magnitudes. Finally, we estimate that terminus position uncertainties are approximately equal to the resolution of the satellite images (±1 pixel or 15–30 m; Carr et al., 2013; McNabb et al., 2015).

Potential biases in dynamic flux and terminus change fluxes were estimated two ways. First, we quantified dynamic flux bias estimates for profiles that used partially interpolated speed and/or thickness cross sections by comparing differences between observed and interpolated values adjacent to data gaps. This bias is typically small ($<2\%$ on average). Second, we estimated biases in bed elevations using the available sonar- and radar-derived bed depths as described in section 3.2 (Figures 2b and S2). The potential systematic overestimation of bed elevations by the M12 and Flotation bedmaps will impact both dynamic flux and terminus change flux estimates. To estimate associated terminus volume change biases, we assume that bed

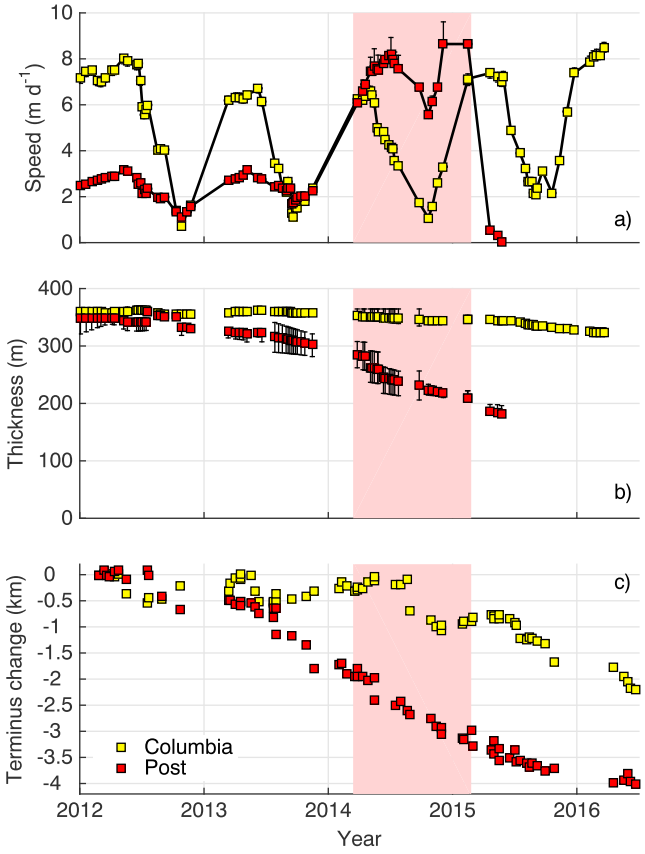

Figure 3. Centerline (a) speed, (b) thickness, and (c) terminus change for Columbia (yellow) and Post (red) glaciers. The speed and thickness data in (a) and (b) are extracted from fluxgate midpoints. In (c), negative terminus change indicates retreat (i.e., decreasing glacier length). The red shading highlights the period of enhanced ice flow and thinning for Post Glacier.

elevation biases along the sonar transect are representative of biases throughout the inner fjord, resulting in a potential systematic underestimation of terminus change flux for Post Glacier by 27% and Columbia Glacier by 11%. The effects of bed elevation biases are smaller for dynamic flux: we find that dynamic flux is potentially underestimated by an average of 21% for Post Glacier due to bed elevation biases but by $<$1% for Columbia Glacier.

Finally, temporal interpolation required to synchronize terminus change flux and dynamic flux in time introduces another source of uncertainty in our frontal ablation estimates. We attempted to minimize this error source by interpolating only dynamic flux, which has a slower and smoother rate of change than terminus volume change and is less prone to aliasing. Although the range in frontal ablation estimates can be large during periods when there is rapid change in dynamic flux between terminus position observations, we note that the impact of this error source is minimized by framing our interpretation around relative changes to fluxes rather than emphasizing the flux magnitude.

4. Results

4.1. Observational Time Series

Figure 3 shows fluxgate centerline speed, surface elevation, and terminus position change time series over the 2012–2016 interval. Although the magnitudes of intra- and interannual variations were greatest along the glaciers' centerlines, the temporal patterns shown in Figure 3 are representative of the entire fast-flowing glacier trunks.

Ice flow speeds across the fluxgates varied intra- and interannually (Figure 3a). Extreme velocity variability (e.g., ~1.5–7.5 m d^{-1} [~550–2750 m yr^{-1}] at C2a) characterizes the near-terminus region of Columbia Glacier, where the fluxgate is located. Up-glacier of the main and east branch confluence, flow variability abruptly decreases, with more consistent, intermediate velocities between the extremes of the spring and fall (e.g., ~4–6 m d^{-1} [~1,450–2,200 m yr^{-1}] at C4a; Figure 4). Similar spatiotemporal velocity variability has been reported at nearby, advancing, Hubbard Glacier, with steady intermediate speeds above a confluence, and widely ranging maxima and minima near the terminus (Stearns et al., 2015).

Through the first half of the record, seasonal minimum speeds (~2 m d^{-1} [~700 m yr^{-1}]) and the timing of seasonality were similar at both glaciers (maxima in May/June, minima in October/November). The primary difference between the two glaciers was the substantially lower range of seasonal ice speeds at Post Glacier. At the end of 2013/beginning of 2014, however, there was a step change in speed at Post Glacier and shortening of the summer-to-fall period of decreased flow speeds (Figure 3, shaded region). The 2015 minimum speeds on Post Glacier were also much lower following this step increase. Similar changes in seasonal variability did not occur at Columbia Glacier.

The thickness time series (Figure 3b) has insufficient temporal sampling to resolve seasonal variations in ice thinning rates. Over interannual time scales, however, the average thinning rate for Post's primary tributary increased from ~26 m yr^{-1} during 2012 through middle 2013 to ~75 m yr^{-1} during 2014 through at least much of 2015. This threefold increase in thinning rate was coincident with a substantial increase in flow speed during 2014 (Figures 3a and 3b). Thinning along Columbia's fast-flowing trunk occurred at a steadier and more gradual rate, with an average thinning rate of ~6.7 m yr^{-1} at the center of the fluxgate (Figure 3b) over the 2012–2016 study period.

On average, Post Glacier retreated at a faster and steadier rate than Columbia Glacier. Through the ~4.5-year study interval, Post Glacier retreated 4.2 km compared to the 2.25-km retreat along the Columbia Glacier

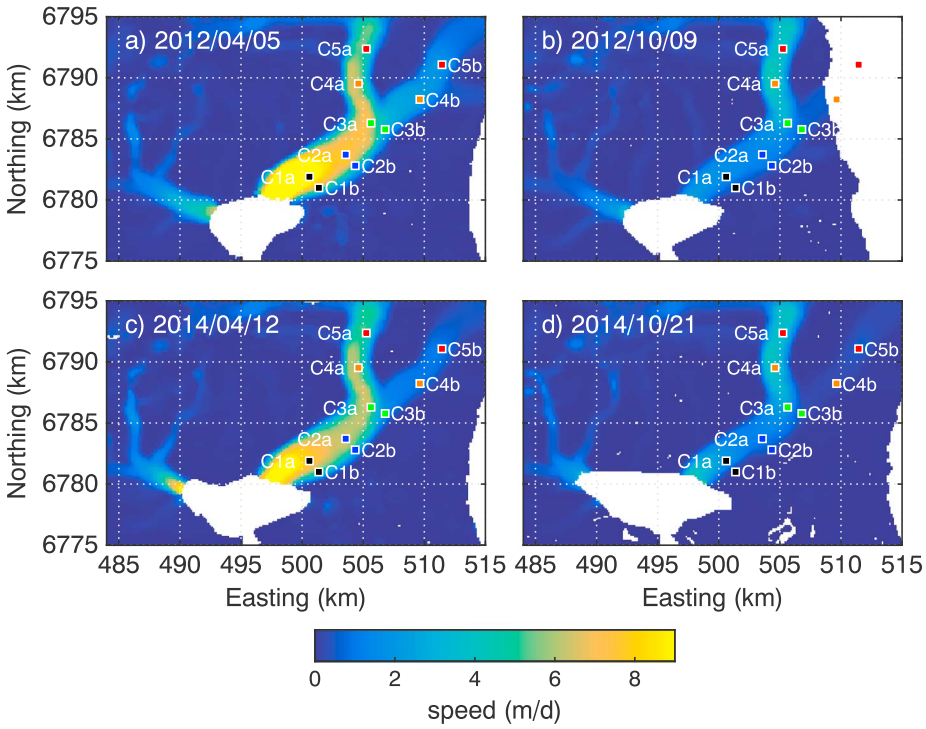

Figure 4. Surface speeds during (a) spring 2012, (b) fall 2012, (c) spring 2014, and (d) fall 2014. Near the glacier termini, seasonal speed maxima generally occur in the spring and minima occur in the fall. Observation dates are listed on each panel.

centerline (Figure 3c). Seasonal patterns were isolated by removing long-term retreat trends with cubic polynomial fits from the terminus position time series (R^2 values of 0.96 and 0.99 for Columbia and Post, respectively). The detrended terminus positions were then fit with smoothing spline functions to resolve seasonal variability while minimizing the high-frequency terminus changes (Figures 5a–5d). The seasonal terminus change curves in Figures 5a–5d indicate that the timing of peak terminus retreat varied between glaciers and through time. There was appreciable seasonality in the Post terminus position from 2012 to 2013, with the glacier occupying its most advanced position in June/July and most retracted position in late fall (Figures 5a and 5b). Over the same time period, we find that terminus position seasonality was similar in amplitude at Columbia, but the timing of seasonality was shifted ~2 months earlier: Columbia reached its most advanced position in April/May and its most-retracted position in August/September (Figures 5a and 5b). Shifts occurred at both glaciers in 2014. At Post, we find a near-constant rate of retreat over seasonal time scales (i.e., no terminus position seasonality) in 2014 and 2015 (Figures 3c and 5c and 5d). At Columbia, after an unusually protracted period during the spring/summer of 2014 over which the glacier occupied a relatively advanced terminus position, the timing of Columbia's seasonal terminus maxima and minima shifted so that the maxima occurred in June/July and minima in late fall/early winter (Figures 5c and 5d).

4.2. Dynamic Flux, Terminus Change Flux, and Frontal Ablation

Figure 6 shows how changes in ice flow speed, thickness, and terminus position combined to produce large intra- and interannual variations in frontal ablation. In general, the terminus change flux at Post Glacier is slightly (~20%) greater than the dynamic flux, reflecting the rapid terminus retreat up the fjord. The nearly 50% reduction of ice thickness along the trunk during the acceleration and retreat ameliorated the impact of acceleration on Post Glacier's dynamic flux; however, frontal ablation still approximately doubled during the speedup. In contrast, dynamic flux dominates frontal ablation for Columbia Glacier over the majority of the study period. The stable terminus at Columbia Glacier resulted in a near-zero terminus-change flux over the 2012–2013 interval. Episodic retreat during the second half of the study provides a substantial contribution to frontal ablation (Figure 6), but these variations were out of phase with dynamic flux and damped seasonal variability of frontal

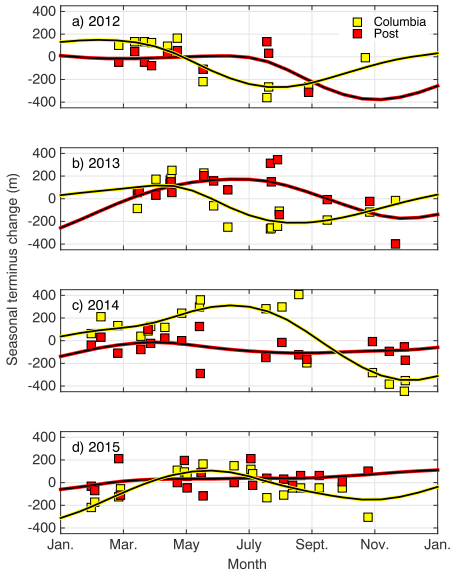

Figure 5. Time series of detrended terminus position change and best fit seasonal terminus change curves for Columbia (yellow) and Post (red) glaciers for (a) 2012, (b) 2013, (c) 2014, and (d) 2015. For both glaciers, these seasonal oscillations were superimposed on a multiyear retreat trend. As in Figure 3c, negative values in all panels indicate more retracted terminus positions.

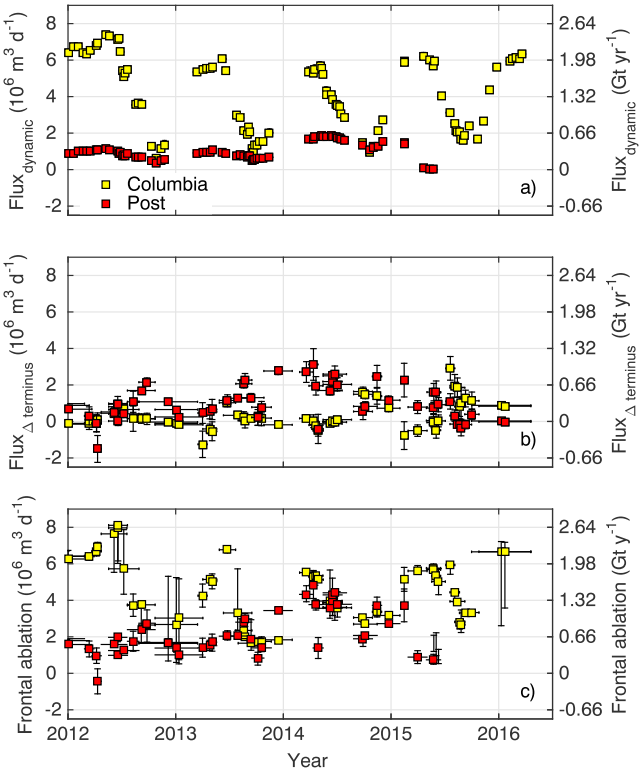

Figure 6. (a) Dynamic flux through the gates in Figure 1a and (b) terminus change flux, where positive values represent mass loss. (c) Frontal ablation, which is the sum of (a) and (b). The horizontal error bars show the observation interval and vertical error bars that represent both random error and potential measurement bias. The error bars in (a) are obscured by the symbols. In all panels, primary *y* axes show fluxes in units of 10^6 m^3 d^{-1} and secondary axes show their equivalents in Gt yr^{-1} assuming an ice density of 900 kg m^{-3}.

ablation. Despite the rapid retreat and flow acceleration at Post Glacier, Columbia Glacier dominated frontal ablation, and thus presumably iceberg discharge, into Columbia Bay throughout most of the study interval.

4.3. Force Balance Time Series

To further investigate seasonal to interannual controls on dynamic change, we constructed 89 force balance maps spanning the ~4.5-year period, with biweekly coverage during some years (see Enderlin et al., 2016 for details of the method, including error estimation). Given the minimal contribution of internal deformation to the fast-flowing regions considered here, we assume that ice flow is dominated by basal sliding and use the depth-integrated force balance equations to estimate longitudinal stress gradients as well as lateral and basal shear stresses (i.e., lateral and basal drag; van der Veen & Whillans, 1989). Although the magnitude of basal drag will be slightly underestimated by our depth-integrated force balance inversion when/where nonnegligible internal deformation exists (van der Veen & Whillans, 1993), spatial patterns in the force balance terms should be accurately captured nonetheless (O'Neel et al., 2005). Near the terminus, however, basal drag will be consistently overestimated because the force balance inversion does not account for longitudinal extension driven by the hydrostatic imbalance between the terminal cliff and ocean water.

Force balance mapping allows us to relate spatial and temporal variations in flow resistance to the physical processes that drive variability. Specifically, our force balance maps reveal a pronounced redistribution of basal drag over seasonal time scales (Figure 7). In the winter and spring months, we resolved near-zero basal drag in broad regions where Columbia Glacier's bed is below sea level (Figures 7a and 7b). Most of the near-terminus ~20-km^2 region with low basal drag experiences a 20–50 kPa increase in basal drag over the course of the late summer and fall months (Figures 7c–7f). As a consequence of this stress redistribution, basal drag decreases upstream and near the lateral margins (negative areas in Figures 7e and 7f). Although force balance estimates are more limited in space and time at Post Glacier due to the relatively poor coverage of the velocity and elevation fields, data from 2012 suggest that pronounced variations in basal drag also occur where the bed is below sea level (Figures 7a, 7c, and 7e). At Post Glacier, however, the region over which we observe seasonality in basal drag is approximately 10-fold smaller than that found at Columbia Glacier.

The full 2-D time series with results for all four force balance terms is presented in the supporting information; here we present extracted values for gravitational driving stress, longitudinal stress gradients, lateral drag, and basal drag at 3.5-km increments along central flowlines of the Columbia's Main and East branches (Figures 1a, 8, and 9) to elucidate the seasonal redistribution of resistive stresses. Force balance time series for Post Glacier are shown in Figure S3 but are not discussed here since they are more limited in space and time than the Columbia force balance results. Following convention, resistive stresses are defined positive when they resist flow (van der Veen, 2013). The relative importance of each resistive stress term (Figures 8 and 9b–9d) can be shown as fractional resistance to the

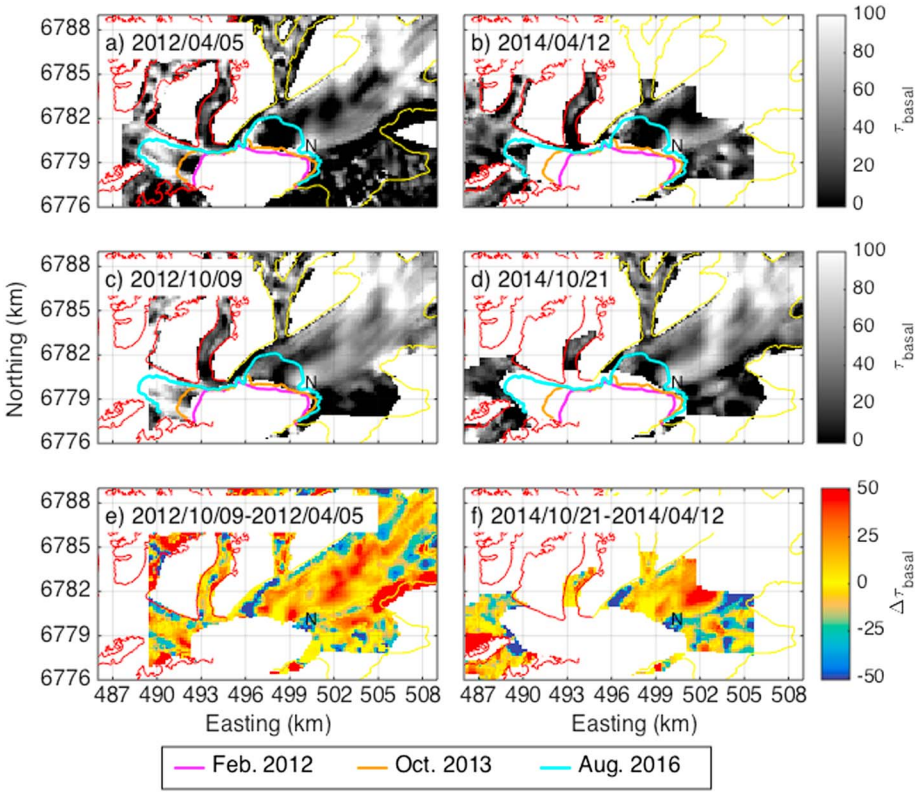

Figure 7. Basal drag maps for (a) spring 2012, (b) spring 2014, (c) fall 2012, (d) fall 2014, (e) the difference between spring and fall 2012, and (f) the difference between the spring and fall 2014. Dates are listed on each panel. For (e) and (f), positive values indicate that basal drag increased from the spring to fall. The "N" in each panel denotes the location of a sticky spot corresponding to the location of a nunatak that has recently emerged from the glacier terminus. The lines in (a)–(d) map terminus positions at the dates defined in the legend.

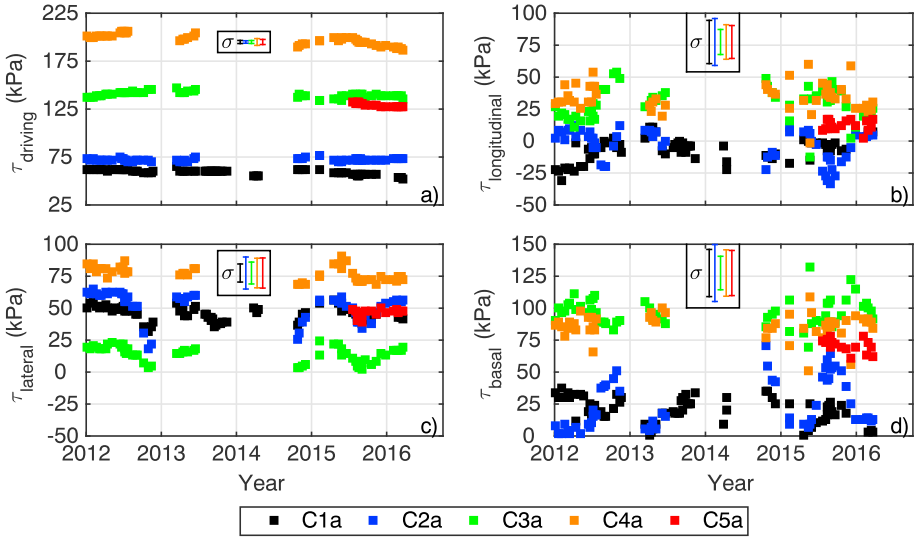

Figure 8. Time series of (a) gravitational driving stress, (b) longitudinal stress, (c) lateral stress, and (d) basal stress for main branch Columbia Glacier. All stresses are in units of kPa, but vertical scaling varies between subplots to highlight temporal variations in each term. The symbol colors identify locations in Figure 1a, with C1a closest to the terminus. The small box in each panel shows the average estimated uncertainty for each site.

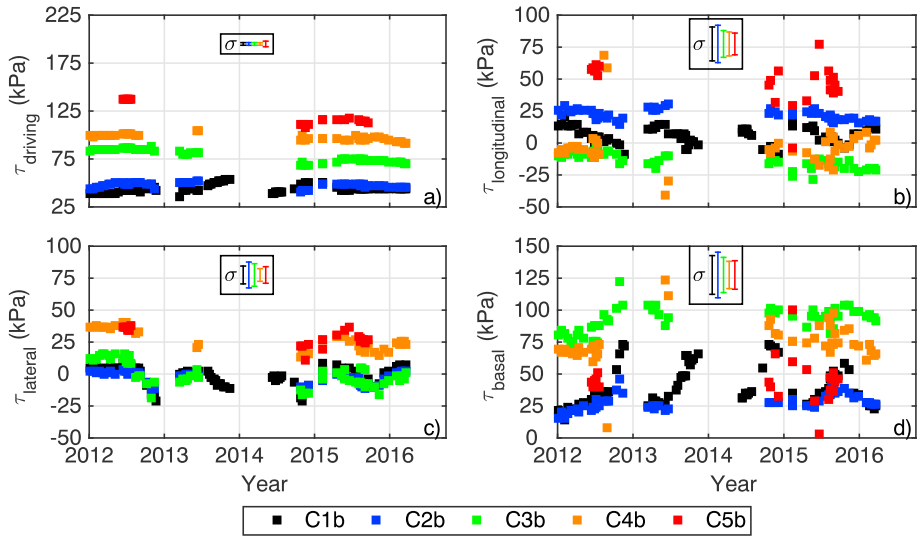

Figure 9. Time series of (a) gravitational driving stress, (b) longitudinal stress, (c) lateral stress, and (d) basal stress for east branch Columbia Glacier. All stresses are in units of kPa, but vertical scaling varies between subplots and to highlight temporal variations in each stress term. The symbol colors identify locations in Figure 1a, with C1b closest to the terminus. The small box in the upper right of each panel shows the average estimated stress uncertainty for each sample site.

driving stress (Figure 10) to help elucidate seasonality of the resistive terms. Where extensional flow occurs (negative longitudinal stresses in Figures 8 and 9), the longitudinal stress gradients complement the driving stress in forcing ice flow. In these regions, values of resistance due to basal drag may exceed 100% of the gravitational driving stress as the lateral and basal stresses must also resist ice flow due to longitudinal extension.

One of the clearest temporal patterns is that the relative contribution of basal drag to ice flow resistance varied both seasonally and along Columbia Glacier. In particular, we find that during spring fast flow, those sites where the bed is grounded below sea level within the main branch (C1a–C3a) had basal drag values of $<$25 kPa (Figure 8d), which is $<$20% of the driving stress (Figure 10e). Here flow resistance was primarily supplied by lateral drag during periods of rapid glacier flow (~50 kPa = ~80% of gravitational driving stress; Figures 8–10). In contrast, during the autumnal periods of deceleration, resistance from lateral drag decreases, with basal drag accounting for a seasonal maximum of ~50% of the driving stress (Figures 8–10). Although basal drag was higher and accounted for a greater percentage of overall flow resistance along the east branch, we observed comparable seasonal changes in basal drag there as well (Figures 10b, 10d, and 10f). Overall, we see that bed topography modulates relative differences in lateral and basal drag; we observe more consistent and higher basal traction in the east branch where the bed elevation is higher and near-zero basal drag where the bed elevation is lowest (main branch sites C1a and C2a). Our observation of minimum basal drag in regions of lowest bed elevation (Figures 2d and 2e), and presumably minimum effective pressures, is consistent with theory (Cuffey & Paterson, 2010).

5. Discussion

5.1. Overview

Retreat, thinning, and flow acceleration (i.e., dynamics) play an important first-order role in mass loss from tidewater glaciers (Enderlin et al., 2014; McNabb et al., 2015; Melkonian et al., 2016; Rignot et al., 2011; Van Wychen et al., 2015). Knowledge of the forcings behind retreat and the magnitude and style of the associated glacier response is critical to successful forecasts of the behavior of ice masses and their contributions to global sea level rise (Joughin, Alley, et al., 2012). Dynamic mass loss occurs through iceberg discharge from the glacier terminus and changes in terminus position (Figure 6). Both of these contributors vary spatially and temporally and are influenced by geometry (i.e., internal instabilities and feedbacks) and environmental forcing.

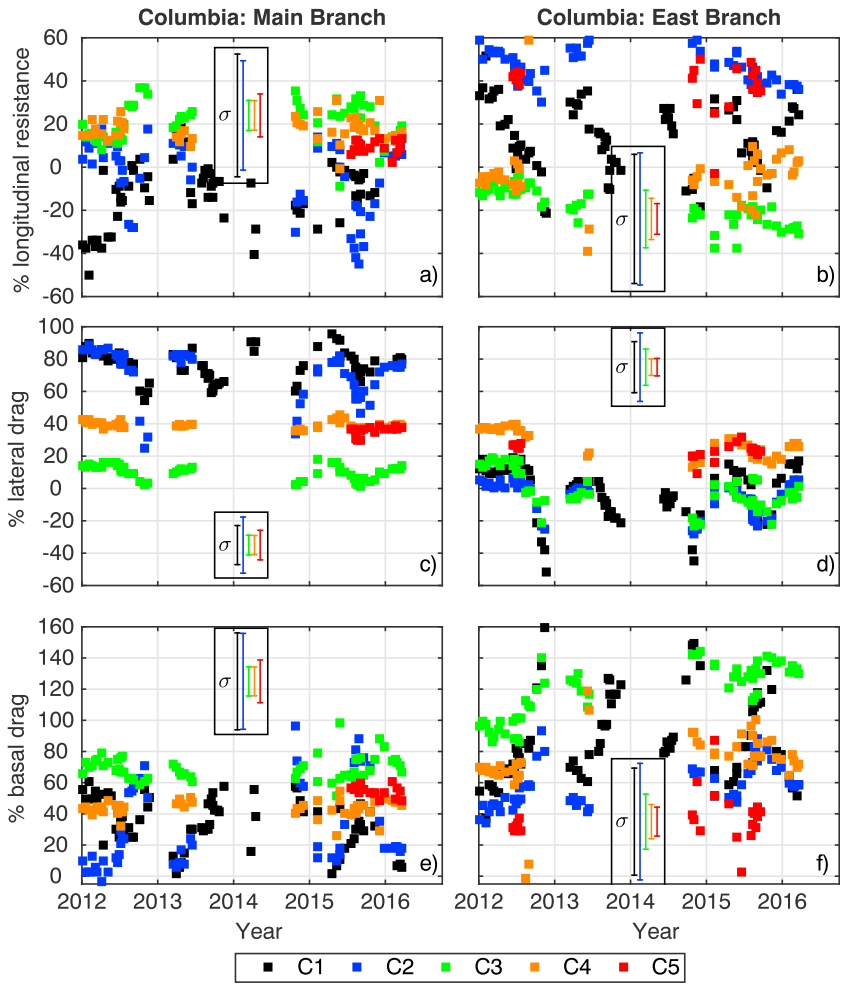

Figure 10. Percentage of gravitational driving stress opposed by (a and b) longitudinal stress gradients, (c and d) lateral stress, and (e and f) basal stress for Columbia. The left and right columns contain results for the glacier's main and east branches, respectively. The negative values indicate that the stress term is acting in the direction of ice flow. For basal stress, values greater than 100% reflect the contribution of longitudinal extension to driving ice flow.

We investigate the controls on dynamic mass loss through detailed examination of the components of frontal ablation and the glacier force balance. The time series of frontal ablation and terminus position reveal whether short-term variations in dynamic mass loss were primarily driven by speed or terminus position change during our study period. When paired with force balance time series, these data also yield insights into the physical mechanisms that likely drive the observed temporal variations in dynamic mass loss.

5.2. The Importance of Environmental Controls

Over the 2012–2016 study interval, our data show that dynamic mass loss from Post Glacier was driven almost equally by dynamic flux and terminus retreat (Figure 6). At Columbia Glacier, dynamic flux accounted for the majority of dynamic mass loss (and its change over time) during the same time period (Figure 6). This difference in the relative importance of dynamic flux and terminus change fluxes can largely be attributed to the pronounced differences in speed and terminus retreat rates. Dynamic flux rates from Post and Columbia are comparable when fluxgate flow speeds are at their annual (fall) minima of ~1–2 m d^{-1}, but dynamic flux for Columbia triples from ~2×10^6 to ~6×10^6 m^3 d^{-1} (~0.7–2.2 km^3 yr^{-1}) during the winter/spring when ice flow speeds reach ~6 m d^{-1} (Figures 3a and 6a). The much greater retreat of the Post terminus means that terminus change fluxes for Post are generally larger than for Columbia over the study period.

We investigated two possible controls on speed seasonality: (1) meltwater-induced evolution of the subglacial drainage network and (2) terminus retreat. Previous observations of Alaskan tidewater glacier speeds suggest that seasonal changes in surface meltwater production alter the subglacial drainage network and thus basal drag (Durkin et al., 2017; McNabb et al., 2015; Ritchie et al., 2008; Stearns et al., 2015). Using a similar TSX-derived record of surface speeds from 2011 to 2016, Vijay and Braun (2017) recently postulated that speed seasonality at Columbia and Post is driven primarily by the evolution of the subglacial drainage network. As in our analysis, they observed that flow speeds reach their seasonal maxima in spring, then rapidly decrease throughout the summer months, reaching their seasonal minima in late fall—typically November (Figure 3b). We further tested this hypothesis by investigating the role of atmospheric forcing on seasonal variations in flow. First, we constructed a proxy record for meltwater forcing from the lapse-rate-derived air temperature record over the 2012–2016 observation period. In each of 4 years and at both glaciers, we find that ice speed at each fluxgate decreases over the course of the melt season (May–November). The timing of the onset of seasonal deceleration is qualitatively linked with positive degree days, such that warm springs are associated with an earlier onset of deceleration. These relationships suggest a link between atmospheric forcing, evolution, and pressurization of the subglacial hydrologic network and effective-pressure controlled basal sliding (Bartholomew et al., 2010; Meier & Post, 1987). Such a link should manifest as seasonal changes in basal lubrication and effective pressure, in phase with velocity variations (O'Neel et al., 2005).

For both glaciers, the seasonal increase in basal traction and the coincident increase in surface air temperatures and meltwater runoff suggest that flow speeds (and dynamic flux) decrease throughout the summer as the result of changes in the subglacial hydrologic network. Specifically, we attribute the seasonal increase in basal drag to an increase in effective pressure brought on by the development of an efficient drainage network over the course of the melt season (Burgess et al., 2013; Schoof, 2010). We hypothesize that the spatial extent of the large seasonal variations in sliding speed and basal drag are governed by glacier geometry and its connection to subglacial hydrology. Large oscillations in speed and basal drag occur below the confluence of the glaciers' largest tributaries, where the bed is below sea level. The confluence of subglacial meltwater from the two tributaries and the low bed elevations, and thus low effective pressures, should promote the seasonal formation of efficient low-pressure conduits that rapidly evacuate meltwater from the near-terminus subglacial drainage network in the summer months.

When we turn our attention to changes in terminus position as a potential driver of seasonality in flow speeds and dynamic flux, our results are consistent with the long-term acceleration of the glacier being driven primarily by unstable terminus retreat (Meier & Post, 1987; O'Neel et al., 2005). Over interannual time scales the glacier accelerates as the terminus retreats, but over seasonal time scales increased ice flow is not necessarily coincident with terminus retreat (Figure 3c). We find that terminus retreat typically occurs from May/June through October/November and is coincident with deceleration rather than acceleration. Since it is actually terminus thickness rather than position that is a more important control on speed, this may simply reflect minor variations in bed slope that our DEMs do not fully resolve. Thus, our data reveal a pattern whereby meltwater flux-driven evolution of the basal hydrological system dominates seasonal flow variability. This behavior is in contrast with observations from some tidewater glaciers in Greenland, where seasonal terminus position oscillations over a retrograde bed slope exert a stronger influence on flow speed than seasonal meltwater-driven changes in subglacial hydrology (Bartholomaus et al., 2016; Cassotto et al., 2015; Howat et al., 2010; Joughin, Smith, et al., 2012). The influence of the terminus is also a nonlinear function of thickness, and Columbia and Post glaciers are on far shallower beds (~200 m) than some Greenlandic glaciers (>600 m). For glaciers in Greenland where melt forcing does dominate, the range of flow speed variability is on the order of tens of percent, versus the several-fold changes observed here (Moon et al., 2014).

Over our study interval, the insensitivity of Columbia Glacier to short-term variations in terminus position suggests that seasonal terminus position fluctuations have a small influence on near-terminus resistive stress relative to those from changes in subglacial effective pressure (described above). The terminus annually retreated over a <3-km^2 area of near-zero basal drag (Figures 7a and 7c), leading to an area-integrated reduction in basal drag that is at least an order of magnitude less than that which occurs as the result of the evolution of the subglacial drainage network (20–50 kPa reduction over ~20 km^2). Likewise, the ~4.5-km^2 region of retreat for Post Glacier (2012–2013) occurred over a deep portion of the fjord associated with low basal drag (Figure 7a magenta and orange lines) and resulted in only a small force balance perturbation. However, once

the terminus began to retreat across the area of initially high (>100 kPa in 2012) basal drag in winter 2014 (Figures 7a–7d), Post Glacier rapidly accelerated and thinned (Figure 3 red shading).

5.3. The Importance of Geometry

Although both glaciers were subjected to the same decadal dynamic history and presumably nearly identical environmental forcing over the study period, the timing of terminus retreat varied between glaciers over both seasonal and interannual time scales. Glaciers are most sensitive to environmental change (i.e., most unstable) when near flotation over a deep bed and terminating on a reverse bed slope (e.g., Brinkerhoff et al., 2017; Carr et al., 2015; Enderlin et al., 2013; Hughes, 1986; Meier & Post, 1987; Porter et al., 2014; Weertman, 1974) or when terminating in broad fjords (e.g., Enderlin et al., 2013; Mercer, 1961). Stability emerges from shallow, well-grounded regions and instability arises when near-buoyancy conditions prevail at the terminus, especially along beds with reverse-slopes (Meier & Post, 1987; Pfeffer, 2007; Schoof, 2007; Vieli et al., 2001).

Our high-resolution time series suggest that the marked variations in the seasonal and multiyear rates of terminus retreat observed at Post and Columbia glaciers are caused by differences in bed geometry and that changes in coupling between dynamics and frontal ablation are geometry dependent. Given invariant bed topography, we would expect that periodic environmental forcings (e.g., seasonal variations in surface meltwater) lead to consistent seasonal periodicity. These climate-forced processes have semipredictable glacier response, with higher frequency (rain, tides, and diurnal melt) forcing terms superposed and potentially occluding seasonal patterns (e.g., Schoof, 2010). However, differences in geometry modulate a glacier's response to environmental change; if a glacier's geometry is such that environmentally forced thinning reduces the gravitational driving stress more than basal drag, the glacier will be relatively insensitive to environmental change (Pfeffer, 2007). Assuming that basal sliding varies as a function of the effective pressure at the glacier base, then the response of a glacier to environmental forcing is strongly dependent on its proximity to flotation (e.g., Enderlin et al., 2013; Pfeffer, 2007). The buoyancy state of the near-terminus region is therefore a critical control on stability; abrupt shifts from stable (i.e., far from buoyancy) to unstable (i.e., near buoyancy) positions may result from long-term dynamic readjustments and/or seasonal oscillations in ice dynamics or environmental forcing.

The strong influence of geometry on terminus position stability and the dynamic response of glaciers to terminus position change are clearly illustrated by Columbia and Post glaciers following their separation in 2010. From 2012 through 2013, the terminus of Post Glacier seasonally advanced and retreated in response to variability in both ice flux and mass removal from the terminus as it retreated onto a relatively shallow shoal (Figures 2e and 6a and 6b). After retreating to the shoal in 2013, its geometry evolved so that it briefly satisfied the stability criterion posed by Pfeffer (2007; Figure 1b black diamond outlines) and dynamic thinning became concentrated near the terminus (Figure 3e). Focused terminus thinning reduced the ice thickness in 2014 to the level at which it no longer satisfied Pfeffer's stability criterion (Figure 1b red diamond outlines and Figure 3b red shading). At that point, inland propagation of thinning resumed in 2014, the terminus retreated into deeper water, and basal drag decreased near the terminus (Figure 7b). The increase in the rate of inland thinning (Figures 1e and 2b) promoted additional rapid retreat that precluded seasonal oscillations in terminus position. By 2016, the retreat rate began to slow and frontal ablation dropped to near zero, likely indicating the glacier reached a stable configuration on a forward sloping bed by the end of the study period.

At Columbia Glacier, we observed differences in the timing of terminus retreat seasonality that we suggest are linked to time varying terminus geometry. From 2012 through 2013, the terminus was grounded across a shallow (<100 m deep) shoal (Figure 2e). Analysis of the Pfeffer (2007) stability criterion indeed reveals that the terminus was stable to perturbations at this time (Figure 1b black squares). In 2014, the terminus retreated from the shoal, likely as the result of a combination of long-term thinning driven by the glacier's multidecadal retreat (O'Neel et al., 2005) and short-term thinning driven by the seasonal retreat of the terminus to a less stable configuration (Figures 1b squares, 2e, and 3b). Although we do not have sufficient DEM coverage to fully substantiate this buoyancy-driven retreat hypothesis, buoyancy-driven calving has been previously shown to strongly control multiyear retreats (Vieli et al., 2001). Importantly, we find that the change in terminus geometry coincided with a 1–2 month delay of seasonal retreat that cannot easily be explained by a change in environmental conditions (Figure 5). A similar delay in the timing of seasonal

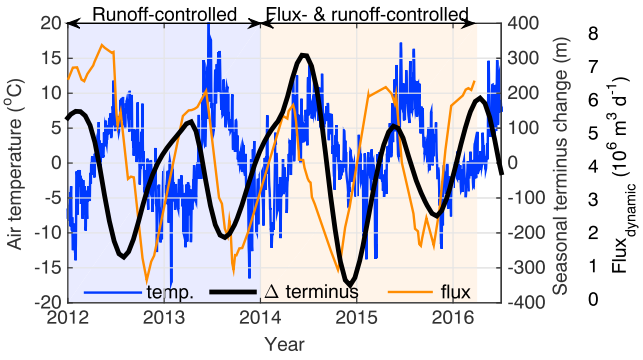

Figure 11. Potential factors controlling the seasonality of Columbia Glacier terminus advance and retreat (black, right *y* axis) include variations in air temperature (blue, left *y* axis) and dynamic flux (orange, right *y* axis). The putative shift in controlling influence on terminus position is labeled.

terminus retreat was observed during Columbia Glacier's retreat from its terminal moraine in the early 1980s (Krimmel, 2001).

Our observations suggest that terminus geometry, that is, whether a glacier is (at least temporarily) stably grounded across a shallow shoal or retreating down a retrograde bed slope, is a first-order dynamic control on the glaciers' response to environmental processes. During 2012–2013, Columbia's terminus was grounded on a shallow shoal. Seasonal retreat began when air temperatures rose above freezing and ceased when temperatures began to decrease in August (Figure 11 black and blue lines). The synchronization between terminus position and air temperature suggests a link between surface melt, submarine melting, and/or calving. Hydrographic observations from nearby Icy Bay indicate that surface meltwater-driven changes in submarine melting may act as the dominant control on seasonal retreat of Alaskan glacier termini (Bartholomaus et al., 2013). Although we do not have the hydrographic observations required to estimate submarine melt rates in Columbia Bay, the observed link between air temperature and terminus position change suggests that seasonal variations in submarine undercutting of the glacier terminus may exert an important control on terminus position at Columbia as well. The effects of seasonal variations in meltwater-driven crevasse hydrofracture on iceberg calving (e.g., Benn et al., 2007) can also be called upon as a potential explanation for the link between seasonal air temperature and terminus position changes.

Interestingly, as Columbia's terminus retreated off the shoal into deeper water in 2014, seasonal changes in terminus position decoupled from changes in air temperature (Figure 11, blue lines). Instead, seasonality in terminus position was best correlated with the dynamic flux (Figure 11, orange lines). As was previously documented by Krimmel (2001), we hypothesize that the ice surface lowers throughout the summer months as the ice flux from the interior progressively decreases (Figures 6a and 11). All else being equal, because near-terminus longitudinal stretching increases with the ice thickness at the terminus (see Nick et al., 2007 and Enderlin et al., 2013 terminus boundary conditions), the magnitude of this seasonal thinning should increase with the bed depth at the terminus. Thus, seasonal changes in ice flux from the interior are more prone to drive terminus retreat via buoyancy-driven calving when the terminus is retreated from a shoal (van der Veen, 1996; Vieli et al., 2001). The hypothesized terminus position dependency on buoyancy-driven summertime calving is supported by the ability of buoyancy-based calving parameterizations to simulate the long-term retreat of Columbia's terminus (Colgan et al., 2012; Nick et al., 2007). Thus, we conclude that the shift in the timing of seasonal terminus retreat is indicative of a shift in the relative sensitivity of the glacier to meltwater and buoyancy effects on calving as the terminus migrated to steeper retrograde slopes and deeper water in the later years.

6. Conclusions and Implications

Using high-resolution time series of terminus position, surface speed, and surface elevation for southcentral Alaska's rapidly retreating Columbia and Post glaciers, we have constructed time series of all frontal ablation and force balance components with subseasonal temporal resolution. We find that a retreating tidewater glacier's long-term dynamic behavior can be dictated by its geometry. However, when geometrical conditions are met, short-term variations in environmental forcing have a major influence on seasonal fluctuations in ice flow speed and terminus position. Importantly, our data suggest that the evolution of the subglacial drainage network, rather than oscillations in terminus position, may act as the primary control on ice flow speed over seasonal time scales. Our data also suggest that the primary controls on seasonal terminus position change can vary with the position of the terminus relative to the bed geometry. For Columbia Glacier, we observe a 1–2 month shift in the timing of seasonal retreat as the glacier retreats from a stabilizing marine shoal. We interpret these changes as an indicator of changes in the importance of buoyancy-driven effects on frontal ablation related to differences in bed slope and water depth at the terminus as the glacier retreats into deeper water.

Thus, our data indicate that there is a give and take between the two principal controls on dynamic mass balance, each taking a turn in controlling the evolution of retreat observed at Columbia Glacier. Although the

relative importance of the principal controls on frontal ablation will undoubtedly vary between glaciers, similar patterns of surface meltwater-driven retreat initiation and subsequent increase in frontal ablation with water depth have also been observed in the Uummannaq region of west Greenland (Rignot et al., 2016). To us, these observations imply that short-term environmental forcings likely play an important role in initiating the retreat of tidewater glaciers from stable positions, but that geometry-driven effects take over once the termini have retreated into deeper water where the ice is close to flotation (Pfeffer, 2007). If the shift in the dominant control on frontal ablation is universally applicable to tidewater glaciers, then these results suggest that confident model-based predictions of tidewater glacier behavior require the use of calving parameterizations that accommodate changes in the primary controls on frontal ablation with glacier retreat.

These results also have important implications for studies that aim to quantify dynamic mass loss and interpret dynamic changes using interannual observations. Long-term studies often rely on records of annual terminus position collected at approximately the same time of year (e.g., Box & Decker, 2011; Carr et al., 2013; Moon & Joughin, 2008), neglecting the role of seasonal cyclicity in contributing to long-term terminus change. However, the Columbia Glacier time series demonstrates nonstationary seasonality, with shifts in peaks of 1–2 months, which could result in substantial over- or underestimates of annual dynamic flux and terminus change fluxes, even relative to other years. Comparable, and even larger shifts in the seasonal timing of retreat have been observed in Greenland (e.g., Joughin et al., 2014; Schild & Hamilton, 2013), indicating that this nonstationarity is not limited to the Columbia system. Thus, we conclude that understanding the relative roles of geometric and environmental forcings is critical to minimize the effects of aliasing on the interpretation of long-term dynamic changes.

Acknowledgments
This analysis was funded by NASA Cryospheric Sciences grant NNX14AH83G awarded to E.M. Enderlin and S. O'Neel. The velocity fields were generated by I. Joughin through U.S. National Science Foundation grant ANT-0424589. WorldView images were distributed by the Polar Geospatial Center at the University of Minnesota (http://www.pgs.umn.edu/imagery/satellite) as part of an agreement between the U.S. National Science Foundation and the U.S. National Geospatial Intelligence Agency Commercial Imagery Program. Geospatial support for this work provided by the Polar Geospatial Center under National Science Foundation Office of Polar Programs awards 1043681 and 1559691. DEMs were generated from WorldView images DigitalGlobe, Inc. imagery using supercomputing resources provided by the University of Maine Advanced Computing Group. Any use of trade, firm, or product names is for descriptive purposes only and does not imply endorsement by the U.S. Government. Terminus position time series from McNabb and Hock (2014) can be accessed using the NASA National Snow and Ice Data Center Distributed Active Archive Center (doi: https://doi.org/10.5067/3OOVUDFK3R0W). The speed maps, DEMs, bed elevation map, force balance maps, and partitioned frontal ablation time series are archived on the Maine DataVerse Network (http://dataverse.acg.maine.edu/dvn/dv/eep).

References

Barclay, D. J., Wiles, G. C., & Calkin, P. E. (2009). Holocene glacier fluctuations in Alaska. *Quaternary Science Reviews*, *28*(21-22), 2034–2048. https://doi.org/10.1016/j.quascirev.2009.01.016

Bartholomaus, T. C., Larsen, C. F., & O'Neel, S. (2013). Does calving matter? Evidence for significant submarine melt. *Earth and Planetary Science Letters*, *380*, 21–30. https://doi.org/10.1016/j.epsl.2013.08.014

Bartholomaus, T. C., Stearns, L. A., Sutherland, D. A., Shroyer, E. L., Nash, J. D., Walker, R. T., et al. (2016). Contrasts in the response of adjacent fjords and glaciers to ice-sheet surface melt in West Greenland. *Annals of Glaciology*, *57*(73), 25–38. https://doi.org/10.1017/aog.2016.19

Bartholomew, I., Nienow, P., Mair, D., Hubbard, A., King, M. A., & Sole, A. (2010). Seasonal evolution of subglacial drainage and acceleration in a Greenland outlet glacier. *Nature Geoscience*, *3*(6), 408–411. https://doi.org/10.1038/ngeo863

Benn, D. I., Warren, C. R., & Mottram, R. H. (2007). Calving processes and the dynamics of calving glaciers. *Earth Science Reviews*, *82*(3-4), 143–179. https://doi.org/10.1016/j.earscirev.2007.02.002

Boldt Love, K., Hallet, B., Pratt, T. L., & O'Neel, S. (2016). Observations and modeling of fjord sedimentation during the 30 year retreat of Columbia Glacier, AK. *Journal of Glaciology*, *62*(234), 778–793. https://doi.org/10.1017/jog.2016.67

Box, J. E., & Decker, D. T. (2011). Greenland marine-terminating glacier area changes: 2000–2010. *Annals of Glaciology*, *52*(59), 91–98. https://doi.org/10.1017/jog.2016.67

Brinkerhoff, D., Truffer, M., & Aschwanden, A. (2017). Sediment transport drives tidewater glacier periodicity. *Nature Communications*, *8*(1), 90. https://doi.org/10.1038/s41467-017-00095-5

Burgess, E. W., Forster, R. R., & Larsen, C. F. (2013). Flow velocities of Alaskan glaciers. *Nature Communications*, *4*(1). https://doi.org/10.1038/ncomms3146

Calkin, P. E., Wiles, G. C., & Barclay, D. J. (2001). Holocene coastal glaciation of Alaska. *Quaternary Science Reviews*, *20*(1-3), 449–461. https://doi.org/10.1016/S0277-3791(00)00105-0

Campbell, R. (2014). Hydrographic Survey of Columbia Bay, October 8–11, 2014. Prince William Sound Regional Citizen's Advisory Council.

Carlson, A. E., Kilmer, Z., Ziegler, L. B., Stoner, J. S., Wiles, G. C., Starr, K., et al. (2017). Recent retreat of Columbia Glacier, Alaska: Millennial context. *Geology*, *45*(6), 547–550. https://doi.org/10.1130/G38479.1

Carr, J. R., Stokes, C., & Vieli, A. (2014). Recent retreat of major outlet glaciers on Novaya Zemlya, Russian Arctic, influenced by fjord geometry and sea-ice conditions. *Journal of Glaciology*, *60*(219), 155–170. https://doi.org/10.3189/2014JoG13J122

Carr, J. R., Stokes, C. R., & Vieli, A. (2017). Threefold increase in marine-terminating outlet glacier retreat rates across the Atlantic Arctic: 1992–2010. *Annals of Glaciology*, *58*(74), 72–91. https://doi.org/10.1017/aog.2017.3

Carr, J. R., Vieli, A., & Stokes, C. (2013). Influence of sea ice decline, atmospheric warming, and glacier width on marine-terminating outlet glacier behavior in Northwest Greenland at seasonal to inter-annual timescales: Controls of outlet glacier behavior. *Journal of Geophysical Research: Earth Surface*, *118*, 1210–1226. https://doi.org/10.1002/jgrf.20088

Carr, J. R., Vieli, A., Stokes, C. R., Jamieson, S. S. R., Palmer, S. J., Christoffersen, P., et al. (2015). Basal topographic controls on rapid retreat of Humboldt Glacier, northern Greenland. *Journal of Glaciology*, *61*(225), 137–150. https://doi.org/10.3189/2015JoG14J128

Cassotto, R., Fahnestock, M., Amundson, J. M., Truffer, M., & Joughin, I. (2015). Seasonal and interannual variations in ice melange and its impact on terminus stability, Jakobshavn Isbræ, Greenland. *Journal of Glaciology*, *61*(225), 76–88. https://doi.org/10.3189/2015JoG13J235

Clarke, G. K. C. (1987). Fast glacier flow: Ice streams, surging, and tidewater glaciers. *Journal of Geophysical Research*, *92*, 8835–8841. https://doi.org/10.1029/JB092iB09p08835

Cogley, G., Beedle, M., Berthier, E., Bolch, T., Burgess, E., Cogley, G., et al. (2015). *GLIMS Glacier Database*. Boulder, CO: National Snow and Ice Data Center. https://doi.org/10.7265/N5V98602

Colgan, W., Pfeffer, W. T., Rajaram, H., Abdalati, W., & Balog, J. (2012). Monte Carlo ice flow modeling projects a new stable configuration for Columbia Glacier, Alaska, c. 2020. *The Cryosphere*, *6*(6), 1395–1409. https://doi.org/10.5194/tc-6-1395-2012

Cuffey, K. M., & Paterson, W. S. (2010). *The physics of glaciers* (4th ed.). Oxford: Elsevier.

Durkin, W. J., Bartholomaus, T. C., Willis, M. J., & Pritchard, M. E. (2017). Dynamic changes at Yahtse Glacier, the most rapidly advancing Tidewater glacier in Alaska. *Frontiers in Earth Science*, *5*(21). https://doi.org/10.3389/feart.2017.00021

Enderlin, E. M., Hamilton, G. S., O'Neel, S., Bartholomaus, T. C., Morlighem, M., & Holt, J. W. (2016). An empirical approach for estimating stress-coupling lengths for marine-terminating glaciers. *Frontiers in Earth Science*, *4*(104). https://doi.org/10.3389/feart.2016.00104

Enderlin, E. M., Howat, I. M., Jeong, S., Noh, M.-J., van Angelen, J. H., & van den Broeke, M. R. (2014). An improved mass budget for the Greenland ice sheet. *Geophysical Research Letters*, *41*, 866–872. https://doi.org/10.1002/2013GL059010

Enderlin, E. M., Howat, I. M., & Vieli, A. (2013). High sensitivity of tidewater outlet glacier dynamics to shape. *The Cryosphere*, *7*(3), 1007–1015. https://doi.org/10.5194/tc-7-1007-2013

Gardner, A. S., Moholdt, G., Scambos, T., Fahnstock, M., Ligtenberg, S., van den Broeke, M., & Nilsson, J. (2018). Increased West Antarctic and unchanged East Antarctic ice discharge over the last 7 years. *The Cryosphere*, *12*(2), 521–547. https://doi.org/10.5194/tc-12-521-2018

Howat, I. M., Ahn, Y., Joughin, I., van den Broeke, M. R., Lenaerts, J. T. M., & Smith, B. (2011). Mass balance of Greenland's three largest outlet glaciers, 2000–2010. *Geophysical Research Letters*, *38*, L12501. https://doi.org/10.1029/2011GL047565

Howat, I. M., Box, J. E., Ahn, Y., Herrington, A., & McFadden, E. M. (2010). Seasonal variability in the dynamics of marine-terminating outlet glaciers in Greenland. *Journal of Glaciology*, *56*(198), 601–613. https://doi.org/10.3189/002214310793146232

Howat, I. M., & Eddy, A. (2011). Multi-decadal retreat of Greenland's marine-terminating glaciers. *Journal of Glaciology*, *57*(203), 389–396. https://doi.org/10.3189/002214311796905631

Hughes, T. (1986). The Jakobshavn effect. *Geophysical Research Letters*, *13*, 46–48. https://doi.org/10.1029/GL013i001p00046

IPCC (2013). Summary for policymakers. In T. F. Stocker, et al. (Eds.), *Climate change 2013: The physical science basis. Contribution of working group I to the fifth assessment report of the intergovern mental panel on climate change* (p. 9). Cambridge: Cambridge University Press.

Jamieson, S. S. R., Vieli, A., Livingstone, S. J., Cofaigh, C. Ó., Stokes, C., Hillenbrand, C.-D., & Dowdeswell, J. A. (2012). Ice-stream stability on a reverse bed slope. *Nature Geoscience*, *5*(11), 799–802. https://doi.org/10.1038/ngeo1600

Joughin, I. (2002). Ice-sheet velocity mapping: A combined interferometric and speckle-tracking approach. *Annals of Glaciology*, *34*, 195–201. https://doi.org/10.3189/172756402781817978

Joughin, I., Alley, R. B., & Holland, D. M. (2012). Ice-sheet response to oceanic forcing. *Science*, *338*(6111), 1172–1176. https://doi.org/10.1126/science.1226481

Joughin, I., Howat, I., Alley, R. B., Ekstrom, G., Fahnestock, M., Moon, T., et al. (2008). Ice-front variation and tidewater behavior on Helheim and Kangerdlugssuaq glaciers, Greenland. *Journal of Geophysical Research*, *113*, F01004. https://doi.org/10.1029/2007JF000837

Joughin, I., Smith, B. E., & Abdalati, W. (2010). Glaciological advances made with interferometric synthetic aperture radar. *Journal of Glaciology*, *56*(200), 1026–1042. https://doi.org/10.3189/002214311796406158

Joughin, I., Smith, B. E., Howat, I. M., Floricioiu, D., Alley, R. B., Truffer, M., & Fahnestock, M. (2012). Seasonal to decadal scale variations in the surface velocity of Jakobshavn Isbrae, Greenland: Observation and model-based analysis. *Journal of Geophysical Research*, *117*, F02030. https://doi.org/10.1029/2011JF002110

Joughin, I., Smith, B. E., Shean, D. E., & Floricioiu, D. (2014). Brief communication: Further summer speedup of Jakobshavn Isbræ. *The Cryosphere*, *8*(1), 209–214. https://doi.org/10.5194/tc-8-209-2014

Krimmel, R.M. (2001). Photogrammetric data set, 1957–2000, and bathymetric measurements for Columbia Glacier, Alaska. United States Geological Survey Water-Resources Investigations Report 01–4089.

McNabb, R. W., & Hock, R. (2014). Alaska tidewater glacier terminus positions, 1948–2012. *Journal of Geophysical Research: Earth Surface*, *119*, 153–167. https://doi.org/10.1002/2013JF002915

McNabb, R. W., Hock, R., & Huss, M. (2015). Variations in Alaska tidewater glacier frontal ablation, 1985–2013. *Journal of Geophysical Research: Earth Surface*, *120*, 120–136. https://doi.org/10.1002/2014JF003276

McNabb, R. W., Hock, R., O'Neel, S., Rasmussen, L. A., Ahn, Y., Braun, M., et al. (2012). Using surface velocities to calculate ice thickness and bed topography: A case study at Columbia Glacier, Alaska, USA. *Journal of Glaciology*, *58*(212), 1151–1164. https://doi.org/10.3189/2012JoG11J249

Meier, M. F., & Post, A. (1987). Fast tidewater glaciers. *Journal of Geophysical Research*, *92*, 9051–9058. https://doi.org/10.1029/JB092iB09p09051

Melkonian, A. K., Willis, M. J., Pritchard, M. E., & Stewart, A. J. (2016). Recent changes in glacier velocities and thinning at Novaya Zemlya. *Remote Sensing of Environment*, *174*, 244–257. https://doi.org/10.1016/j.rse.2015.11.001

Mercer, J. (1961). The response of fjord glaciers to changes in the firn limit. *Journal of Glaciology*, *10*(29), 850–858.

Moon, T., & Joughin, I. (2008). Changes in ice front position on Greenland's outlet glaciers from 1992 to 2007. *Journal of Geophysical Research*, *113*, F02022. https://doi.org/10.1029/2007JF000927

Moon, T., Joughin, I., Smith, B., van den Broeke, M. R., van de Berg, W. J., Noël, B., & Usher, M. (2014). Distinct patterns of seasonal Greenland glacier velocity. *Geophysical Research Letters*, *41*, 7209–7216. https://doi.org/10.1002/2014GL061836

Mouginot, J., Rignot, E., & Scheuchl, B. (2014). Sustained increase in ice discharge from the Amundsen Sea Embayment, West Antarctica, from 1973 to 2013. *Geophysical Research Letters*, *41*, 1576–1584. https://doi.org/10.1002/2013GL059069

Nick, F. M., van der Veen, C. J., & Oerlemans, J. (2007). Controls on advance of tidewater glaciers: Results from numerical modeling applied to Columbia Glacier. *Journal of Geophysical Research*, *112*, F03S24. https://doi.org/10.1029/2006JF000551

O'Neel, S., Pfeffer, W. T., Krimmel, R., & Meier, M. (2005). Evolving force balance at Columbia Glacier, Alaska, during its rapid retreat. *Journal of Geophysical Research*, *110*, F03012. https://doi.org/10.1029/2005JF000292

Pfeffer, W. T. (2007). A simple mechanism for irreversible tidewater glacier retreat. *Journal of Geophysical Research*, *112*, F03S25. https://doi.org/10.1029/2006JF000590

Porter, D. F., Tinto, K. J., Boghosian, A., Cochran, J. R., Bell, R. E., Manizade, S. S., & Sonntag, J. G. (2014). Bathymetric control of tidewater glacier mass loss in Northwest Greenland. *Earth and Planetary Science Letters*, *401*, 40–46. https://doi.org/10.1016/j.epsl.2014.05.058

Post, A. (1975). Preliminary hydrography and historic terminal changes of Columbia Glacier, Alaska. United States Geological Survey Hydrologic Atlas 559.

Post, A., O'Neel, S., Motyka, R. J., & Streveler, G. (2011). A complex relationship between calving glaciers and climate. *EOS. Transactions of the American Geophysical Union*, *92*(37), 305–306. https://doi.org/10.1029/2011EO370001

Rasmussen, L.A. (1989). Surface velocity variations of the lower part of Columbia Glacier, Alaska, 1977–1981. United States Geological Survey Professional Paper 1258- H.

Rasmussen, L. A., Conway, H., Krimmel, R. M., & Hock, R. (2011). Surface mass balance, thinning and iceberg production, Columbia Glacier, Alaska, 1948–2007. *Journal of Glaciology*, *57*(203), 431–440. https://doi.org/10.3189/002214311796905532

Rignot, E., Mouginot, J., Larsen, C. F., Gim, Y., & Kirchner, D. (2013). Low-frequency radar sounding of temperate ice masses in southern Alaska. *Geophysical Research Letters*, *40*, 5399–5405. https://doi.org/10.1002/2013GL057452

Rignot, E., Velicogna, I., van den Broeke, M. R., Monaghan, A., & Lenaerts, J. T. M. (2011). Acceleration of the contribution of the Greenland and Antarctic ice sheets to sea level rise. *Geophysical Research Letters*, *38*, L05503. https://doi.org/10.1029/2011GL046583

Rignot, E., Xu, Y., Menemenlis, D., Mouginot, J., Scheuchl, B., Li, X., et al. (2016). Modeling of ocean-induced ice melt rates of five west Greenland glaciers over the past two decades. *Geophysical Research Letters*, *43*, 6374–6382. https://doi.org/10.1002/2016GL068784

Ritchie, J. B., Lingle, C. S., Motyka, R. J., & Truffer, M. (2008). Seasonal fluctuations in the advance of a tidewater glacier and potential causes: Hubbard Glacier, Alaska, USA. *Journal of Glaciology*, *54*(186), 401–411. https://doi.org/10.3189/002214308785836977

Rott, H., Müller, F., Nagler, T., & Floricioiu, D. (2011). The imbalance of glaciers after disintegration of Larsen-B ice shelf, Antarctic Peninsula. *The Cryosphere*, *5*(1), 125–134. https://doi.org/10.5194/tc-5-125-2011

Schild, K. M., & Hamilton, G. S. (2013). Seasonal variations of outlet glacier terminus position in Greenland. *Journal of Glaciology*, *59*(216), 759–770. https://doi.org/10.3189/2013JoG12J238

Schoof, C. (2007). Ice sheet grounding line dynamics: Steady states, stability, and hysteresis. *Journal of Geophysical Research*, *112*, F03S28. https://doi.org/10.1029/2006JF000664

Schoof, C. (2010). Ice-sheet acceleration driven by melt supply variability. *Nature*, *468*(7325), 803–806. https://doi.org/10.1038/nature09618

Shean, D. E., Alexandrov, O., Moratto, Z. M., Smith, B. E., Joughin, I. R., Porter, C., & Morin, P. (2016). An automated, open-source pipeline for mass production of digital elevation models (DEMs) from very-high-resolution commercial stereo satellite imagery. *ISPRS Journal of Photogrammetry and Remote Sensing*, *116*, 101–117. https://doi.org/10.1016/j.isprsjprs.2016.03.012

Stearns, L. A., Hamilton, G. S., van der Veen, C. J., Finnegan, D. C., O'Neel, S., Scheick, J. B., & Lawson, D. E. (2015). Glaciological and marine geological controls on terminus dynamics of Hubbard Glacier, Southeast Alaska. *Journal of Geophysical Research: Earth Surface*, *120*, 1065–1081. https://doi.org/10.1002/2014JF003341

van den Broeke, M. R., Enderlin, E. M., Howat, I. M., Munneke, P. K., Noël, B. P. Y., van de Berg, W. J., et al. (2016). On the recent contribution of the Greenland ice sheet to sea level change. *The Cryosphere*, *10*(5), 1933–1946. https://doi.org/10.5194/tc-10-1933-2016

van der Veen, C. J. (1996). Tidewater calving. *Journal of Glaciology*, *42*(141), 375–385. https://doi.org/10.1017/S0022143000004226

van der Veen, C. J. (2013). *Fundamentals of glacier dynamics*. Boca Raton, FL: CRC Press. https://doi.org/10.1201/b14059

van der Veen, C. J., & Whillans, I. M. (1989). Force budget: I. Theory and numerical methods. *Journal of Glaciology*, *35*(119), 53–60. https://doi.org/10.3189/002214389793701581

van der Veen, C. J., & Whillans, I. M. (1993). Location of mechanical controls on Columbia glacier, Alaska, U.S.A., prior to its rapid retreat. *Arctic and Alpine Research*, *25*(2), 99–105. https://doi.org/10.2307/1551545

Van Wychen, W., Burgess, D. O., Gray, L., Copland, L., Sharp, M., Dowdeswell, J. A., & Benham, T. J. (2015). Glacier velocities and dynamic ice discharge from the Queen Elizabeth Islands, Nunavut, Canada. *Geophysical Research Letters*, *52*, 980–989. https://doi.org/10.1139/cjes-2015-0087

Vancouver, G. (1798). *A voyage of discovery to the North Pacific Ocean, and round the world*. London: G.G. & J. Robinson and J. Edwards.

Vieli, A., Funk, M., & Blatter, H. (2001). Flow dynamics of tidewater glaciers: A numerical modelling approach. *Journal of Glaciology*, *47*(159), 595–606. https://doi.org/10.3189/172756501781831747

Vijay, S., & Braun, M. H. (2017). Seasonal and interannual variability of Columbia Glacier, Alaska (2011–2016): Ice velocity, mass flux, surface elevation and front position. *Remote Sensing*, *9*(6), 635. https://doi.org/10.3390/rs9060635

Walter, F., O'Neel, S., McNamara, D., Pfeffer, W. T., Bassis, J. N., & Fricker, H. A. (2010). Iceberg calving during transition from grounded to floating ice: Columbia Glacier, Alaska. *Geophysical Research Letters*, *37*(15), L15501. https://doi.org/10.1029/2010GL043201

Weertman, J. (1974). Stability of the junction of an ice sheet and ice shelf. *Journal of Glaciology*, *13*(67), 3–11. https://doi.org/10.1017/S0022143000023327